



**University of
Zurich**^{UZH}

**Zurich Open Repository and
Archive**

University of Zurich
Main Library
Strickhofstrasse 39
CH-8057 Zurich
www.zora.uzh.ch

Year: 2013

General equation for the differential pathlength factor of the frontal human head depending on wavelength and age

Scholkmann, Felix; Wolf, Martin

Abstract: Continuous-wave near-infrared spectroscopy and near-infrared imaging enable the measurement of relative concentration changes in oxy- and deoxyhemoglobin and thus hemodynamics and oxygenation. The accuracy of determined changes depends mainly on the modeling of the light transport through the probed tissue. Due to the highly scattering nature of tissue, the light path is longer than the source-detector separation (d). This is incorporated in modeling by multiplying d by a differential pathlength factor (DPF) which depends on several factors such as wavelength, age of the subject, and type of tissue. In the present work, we derive a general DPF equation for the frontal human head, incorporating dependency on wavelength and age, based on published data. We validated the equation using different data sets of experimentally determined DPFs from six independent studies.

DOI: <https://doi.org/10.1117/1.JBO.18.10.105004>

Posted at the Zurich Open Repository and Archive, University of Zurich

ZORA URL: <https://doi.org/10.5167/uzh-89593>

Journal Article

Published Version

Originally published at:

Scholkmann, Felix; Wolf, Martin (2013). General equation for the differential pathlength factor of the frontal human head depending on wavelength and age. *Journal of Biomedical Optics*, 18(10):105004.

DOI: <https://doi.org/10.1117/1.JBO.18.10.105004>

General equation for the differential pathlength factor of the frontal human head depending on wavelength and age

Felix Scholkmann and Martin Wolf

University Hospital Zurich, Biomedical Optics Research Laboratory, Division of Neonatology, 8091 Zurich, Switzerland

Abstract. Continuous-wave near-infrared spectroscopy and near-infrared imaging enable the measurement of relative concentration changes in oxy- and deoxyhemoglobin and thus hemodynamics and oxygenation. The accuracy of determined changes depends mainly on the modeling of the light transport through the probed tissue. Due to the highly scattering nature of tissue, the light path is longer than the source–detector separation (d). This is incorporated in modeling by multiplying d by a differential pathlength factor (DPF) which depends on several factors such as wavelength, age of the subject, and type of tissue. In the present work, we derive a general DPF equation for the frontal human head, incorporating dependency on wavelength and age, based on published data. We validated the equation using different data sets of experimentally determined DPFs from six independent studies. © The Authors.

Published by SPIE under a Creative Commons Attribution 3.0 Unported License. Distribution or reproduction of this work in whole or in part requires full attribution of the original publication, including its DOI. [DOI: [10.1117/1.JBO.18.10.105004](https://doi.org/10.1117/1.JBO.18.10.105004)]

Keywords: continuous-wave near-infrared spectroscopy; differential pathlength factor.

Paper 130483R received Jul. 10, 2013; revised manuscript received Sep. 6, 2013; accepted for publication Sep. 19, 2013; published online Oct. 11, 2013.

1 Introduction

By shining near-infrared (~650 to 950 nm) light into tissue and measuring the diffuse reflected light at different wavelengths (λ), continuous-wave (CW) near-infrared spectroscopy (NIRS) and imaging (NIRI) enable the determination of concentration changes in oxy- and deoxyhemoglobin ([O₂Hb], [HHb]), which are related to changes in hemodynamics and oxygenation.^{1,2} NIRS refers to a measurement at a single position (i.e., one light-path), whereas NIRI measures simultaneously at different positions.

Light transportation through tissue is a complex process. In a first approximation, it can be modeled using the modified Lambert–Beer law³ given as

$$I(\lambda) = I_0(\lambda)e^{-\mu_a(\lambda)d\text{DPF}(\lambda)+G(\lambda)}, \quad (1)$$

where $I(\lambda)$ is the measured wavelength-dependent diffuse reflected light intensity, $I_0(\lambda)$ is the incident light intensity, $\mu_a(\lambda)$ is the absorption coefficient of the probed tissue, d is the distance between the positions of incident and measured light, i.e., the source–detector separation, $\text{DPF}(\lambda)$ the differential pathlength factor (DPF), and $G(\lambda)$ is a wavelength-, medium-, and geometry-dependent constant. The term $d\text{DPF}(\lambda)$ corresponds to the mean light propagation distance in the medium, i.e., the parameter $\text{DPF}(\lambda)$ is a scaling factor that indicates how many times farther than d the detected light has traveled.

Based on the diffusion equation for modeling light transport through a homogeneous semi-infinite medium, it can be shown that the DPF depends on $\mu_a(\lambda)$, the reduced scattering coefficient $\mu'_s(\lambda)$, and d .^{4,5}

$$\begin{aligned} \text{DPF}(\lambda) &= \frac{1}{2} \left(\frac{3\mu'_s(\lambda)}{\mu_a(\lambda)} \right)^{1/2} \left[1 - \frac{1}{(1 + d(3\mu_a(\lambda)\mu'_s(\lambda))^{1/2})} \right] \\ &\approx \frac{1}{2} \left(\frac{3\mu'_s(\lambda)}{\mu_a(\lambda)} \right)^{1/2}. \end{aligned} \quad (2)$$

Consequently, $\text{DPF}(\lambda)$ increases with μ'_s and decreases with μ_a . The dependence of DPF on the source–detector separation (d) is crucial to be considered for small d values, but for $d > 2.5$ cm, the DPF is virtually independent of d .^{6,7} From the mathematical point of view, the dependence of d on the DPF is negligible when the inequality $d\sqrt{3\mu_a\mu'_s} \gg 1$ holds.⁸ Since Eq. (2) is only valid for a homogeneous semi-infinite medium and since the brain is inhomogeneous, the equation only gives an approximation of the real situation in human brain tissue. However, the conclusion about the dependence of the DPF on μ'_s and μ_a remains true. For biological tissue, $\text{DPF}(\lambda)$ is generally in the range of 3 to 6. The DPF value affects the magnitude of the calculated concentration changes of chromophores in the tissue (i.e., [O₂Hb], [HHb]). For CW-NIRS/NIRI, the concentration changes are often determined based on consecutive measurements of $I(\lambda)$ and applying Eq. (1), whereas $\mu_a(\lambda)$ is given as the sum of the specific absorption coefficients $\alpha(\lambda)$, of O₂Hb and HHb, times the concentration c : $\mu_a(\lambda) = c(\text{O}_2\text{Hb})\alpha(\text{O}_2\text{Hb}, \lambda) + c(\text{HHb})\alpha(\text{HHb}, \lambda)$. Using a wrong wavelength dependence of DPF leads to crosstalk similar to using a wrong $\alpha(\lambda)$ value.^{9,10} CW-NIRS cannot measure the actual value of $\text{DPF}(\lambda)$ which must be estimated according to tabulated values. Frequency-domain (FD) or time-domain NIRS/NIRI does not need the DPF to calculate the concentration changes, and these techniques are able to measure the μ_a directly.^{3,11–13} Another solution is to measure the DPF by employing an optical pathlength meter as developed by Tullis and Delpy¹⁴ or to determine continuously the DPF with CW-NIRS by extended Kalman filtering and dynamic system modeling.⁹

In 1996, Duncan et al.¹⁵ showed in a seminal paper that the DPF depends on the age of the subjects. The older the

Address all correspondence to: Felix Scholkmann, University Hospital Zurich, Biomedical Optics Research Laboratory, Frauenklinikstrasse 10, 8091 Zurich, Switzerland. Tel: +41 44 2559326; Fax: +41 44 255 4442; E-mail: Felix.Scholkmann@usz.ch

subject, the larger the DPF. Physiological reasons for the age dependence of the DPF can be attributed to different developmental or aging processes in the human brain, such as the change in intracranial volume (increase from birth to adolescence; decrease after ~50 years of age),^{16,17} myelination (exponential increase over the first 3 years of life; myelin: strong scatterer),¹⁸ gray matter (GM) and white matter (WM) properties (after adulthood onwards: reduction in GM volume and deterioration in WM microstructure),¹⁹ cerebral blood flow and volume (global decrease, ~0.5%/year, due to aging),²⁰ cerebrospinal fluid layer thickness (increase with advanced age),²¹ or cortical thickness, bone mineral content, and cortical bone density (decrease starting from adulthood on).²²

Duncan et al.¹⁵ measured the DPF of 283 subjects (137 male, 146 female, age: 1 day to 50 years) for four different wavelengths (690, 744, 807, and 832 nm) by a FD-NIRS system with a d of 4.3 cm. The optode was placed on the left frontal region (adults) and on the left or right frontotemporal region (on neonates). By using a least squares fitting method, they derived four equations that relate the DPF with age (A):

$$\text{DPF}(\lambda = 690 \text{ nm}, A) = 5.38 + 0.049 A^{0.877}, \quad (3)$$

$$\text{DPF}(\lambda = 744 \text{ nm}, A) = 5.11 + 0.106 A^{0.723}, \quad (4)$$

$$\text{DPF}(\lambda = 807 \text{ nm}, A) = 4.99 + 0.067 A^{0.814}, \quad (5)$$

$$\text{DPF}(\lambda = 832 \text{ nm}, A) = 4.67 + 0.062 A^{0.819}. \quad (6)$$

Since the CW-NIRS/NIRI devices also apply wavelengths other than those employed by Duncan et al.,¹⁵ a general equation modeling the DPF as a variable depending simultaneously on age and wavelength would be desirable. Surprisingly, no such equation has been published to date to the best of our knowledge. The aim of the present work was (1) to derive such an equation and (2) to compare its predictions to various published values of measured DPF.

2 Derivation and Validation of the General Equation

2.1 Derivation: Nonlinear Least Squares Surface Fitting

The general equation relating the DPF with age and wavelength is based on Eqs. (3)–(6).

All data processing was performed using MATLAB (version 2008b, The MathWorks, Natick, Massachusetts). To derive the formula, the general mathematical type of surface equation was first determined. Therefore, the DPF (A) dependence was modeled as power law, $\text{DPF}(A) = \alpha + \beta A^\gamma$, according to Eqs. (3)–(6). The $\text{DPF}(\lambda)$ equation was modeled as a cubic function, $\text{DPF}(\lambda) = \delta \lambda^3 + \varepsilon \lambda^2 + \zeta \lambda + \eta$, since this ensures that the function fits to all four wavelengths [see Fig. 1(c)]. A higher polynomial degree than three would cause overfitting since only four data points are available.

Thus, the surface to be fitted to the data was defined as

$$\text{DPF}(\lambda, A) = \alpha + \beta A^\gamma + \delta \lambda^3 + \varepsilon \lambda^2 + \zeta \lambda. \quad (7)$$

All values obtained by evaluating Eqs. (3)–(6) for $A = 0, 1, \dots, 50$ were fitted by a robust nonlinear least squares fitting with the least absolute residuals (LAR) method²³ and the Levenberg–Marquardt algorithm (LMA).^{24,25} The LAR method is a version of the least sum of squares residuals fitting method based on minimizing the (constrained) sum of the absolute residuals, in comparison to ordinary least squares (OLS) that minimize the sum of squared residuals. LAR has the advantage over OLS of being robust against deviations from the normality assumption of the data. LMA is a cross between the Gauss–Newton algorithm and the steepest descent method; it has the advantage of being robust and iteratively more efficient.

The following parameter values were obtained: $\alpha = 223.3$, $\beta = 0.05624$, $\gamma = 0.8493$, $\delta = -5.723 \times 10^{-7}$, $\varepsilon = 0.001245$, and $\zeta = -0.9025$. The goodness-of-fit statistics obtained were: summed squared of residuals: 0.09668, R-square: 0.9983, adjusted R-square: 0.9983, and root mean squared error (RMSE): 0.0221. These values indicate an excellent fit of the surface to the empirical data. An illustration of the determined $\text{DPF}(\lambda, A)$ function can be seen in Fig. 2.

2.2 Validation of the General Equation

In order to validate the derived general $\text{DPF}(\lambda, A)$ Eq. (7), it was compared to (1) the results of Eqs. (3)–(6) and (2) five data sets of DPFs measured in independent studies.^{6,26–29} Due to the fact that the DPF depends on tissue type, only DPF measurements of the forehead (frontal or frontotemporal) were used for the validation to ensure a homogeneous sample. In addition, only DPF values where $d > 2.5$ cm holds were included since this ensures a value

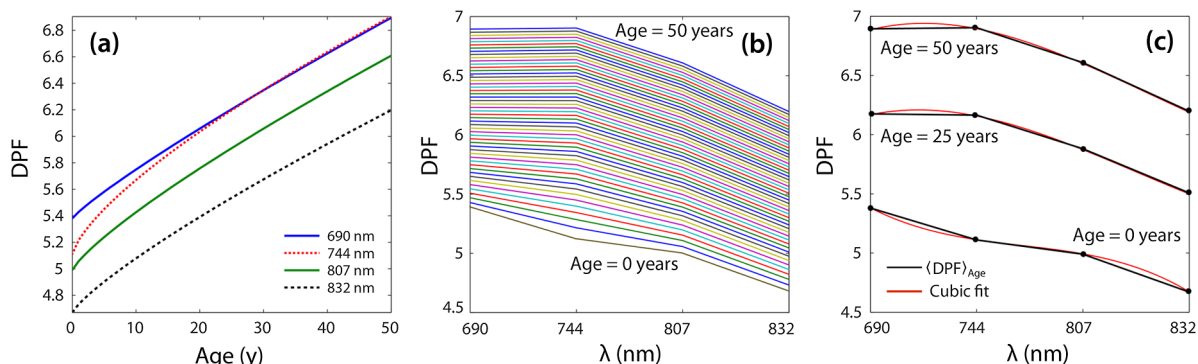


Fig. 1 (a) $\text{DPF}(A)$ for all ages (0 to 50 years) according to Eqs. (3)–(6). (b) $\text{DPF}(\lambda)$ for each age. (c) Exemplary visualization of the cubic fit for three age groups (0, 25, and 50 years).

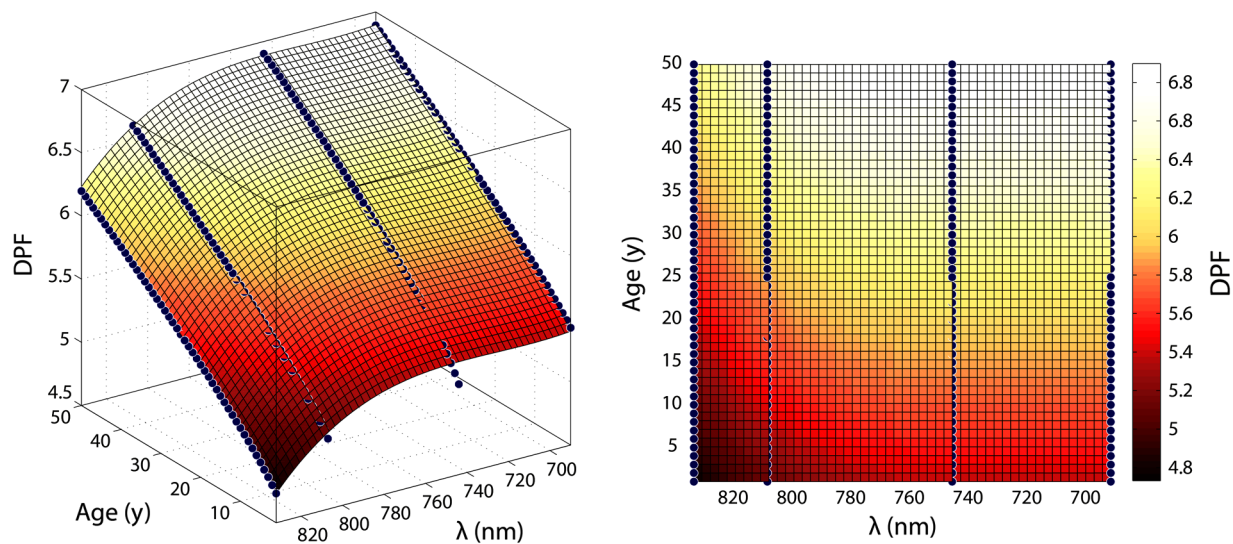


Fig. 2 Visualization of the derived $DPF(\lambda, A)$ equation for the age values 0 to 50 years, and the wavelength values 690 to 832 nm. The surface is shown from two different perspectives.

independent of d .⁶ Table 1 lists the details of the six studies employed in our validation.

The comparison of the values obtained by the general $DPF(\lambda, A)$ equation with the values obtained by Eqs. (3)–(6) revealed a good agreement: $DPF(\lambda, A)$ versus Eq. (3), RMSE: 0.0320; versus Eq. (4), RMSE: 0.0545; versus Eq. (5), RMSE: 0.0311; versus Eq. (6), RMSE: 0.0348.

As expected, the comparison with the different data sets of measured DPFs also revealed a good agreement in general (see Fig. 3). If the predicted value was inside the standard deviation (SD) or quartiles (first to third) of the value measured, we defined this as a correct prediction. The predicted DPF values agree with the measured ones for the data set of Duncan et al.²⁶ and Cooper et al.²⁷ For the van der Zee et al.⁶ data set, the

Table 1 Experimentally obtained differential pathlength factor (DPF) values used for the validation of the general formula.^a

References	Subjects	DPF	
van der Zee et al. ⁶	OP: frontal (adults), frontotemporal (neonates); SDS: > 2.5 cm. (i) Adults; $n = 10$; age (years): 26 (22 to 54). (ii) Preterm (postmortem) neonates; $n = 10$; GA (weeks): 30.6 ± 5.4	(i) Adults: 5.93 ± 0.42 (761 nm)	(ii) Neonates: 3.85 ± 0.57 (783 nm)
Essenpreis et al. ³⁰	OP: frontal (adults and neonate); SDS: 4 cm. (i) Adults; $n = 7$; age (years): 28 (23 to 55). (ii) Neonate (postmortem) ^b ; $n = 1$; GA (weeks): 41	(i) Adults: 6.59 (740 nm) 5.82 (840 nm)	(ii) Neonates: 4.17 (735 nm) 4.19 (840 nm)
Duncan et al. ²⁶	OP: frontal (adults), frontotemporal (neonates), SDS: 4.3 cm. (i) Adults; $n = 100$; age: 33 (21 to 59). (ii) Neonates; $n = 35$; GA (weeks): 40 (35 to 42); age (days): 2 (0 to 16)	(i) Adults 6.51 ± 1.13 (690 nm) 6.53 ± 0.99 (744 nm) 6.26 ± 0.88 (807 nm) 5.86 ± 0.98 (832 nm)	(ii) Neonates 5.38 ± 0.49 (690 nm) 5.11 ± 0.48 (744 nm) 4.99 ± 0.45 (807 nm) 4.67 ± 0.65 (832 nm)
Cooper et al. ²⁷	OP: frontotemporal SDS: 4.9 cm. Neonates; $n = 19$; GA (weeks): 34 (23 to 38); age (days): 21 (1.4 to 23)		4.66 ± 1.06 (730 nm) 3.91 ± 0.75 (830 nm)
Zhao et al. ²⁸	OP: (i) frontal, (ii) frontotemporal; SDS: 3.0 cm. Adults, $n = 11$, age (years): 33 (22 to 53)	(i) Frontal: ^b 7.5 (759 nm) 7.25 (799 nm) 7.0 (834 nm)	(ii) Frontotemporal: ^c 6.5 (759 nm) 6.25 (799 nm) 6.25 (834 nm)
Bonnéry et al. ²⁹	OP: frontal; SDS: 3.0. (i) Adults; $n = 19$; age (years): 24.4 ± 2.5 . (ii) Adults; $n = 23$; age (years): 67.6 ± 2.9	(i) Adults (young): 6.2 (5.6–6.9) (690 nm) 5.8 (5.2–6.1) (830 nm)	(ii) Adults (old): 6.9 (6.2–7.3) (690 nm) 6.1 (5.8–6.8) (830 nm)

^aGA: gestational age, OP: optode placement, SDS: source-detector separation. Data were reported as either mean \pm standard deviation (SD) or median (first quantile, third quantile), or median (span).

^bOnly the data for the neonate with a gestational age of 47 weeks was used since the other reported neonate (gestational age: 27 weeks) was a preterm one with a bilateral hemorrhagic parenchymal infection.

^cFrom the authors recommended general values to use.

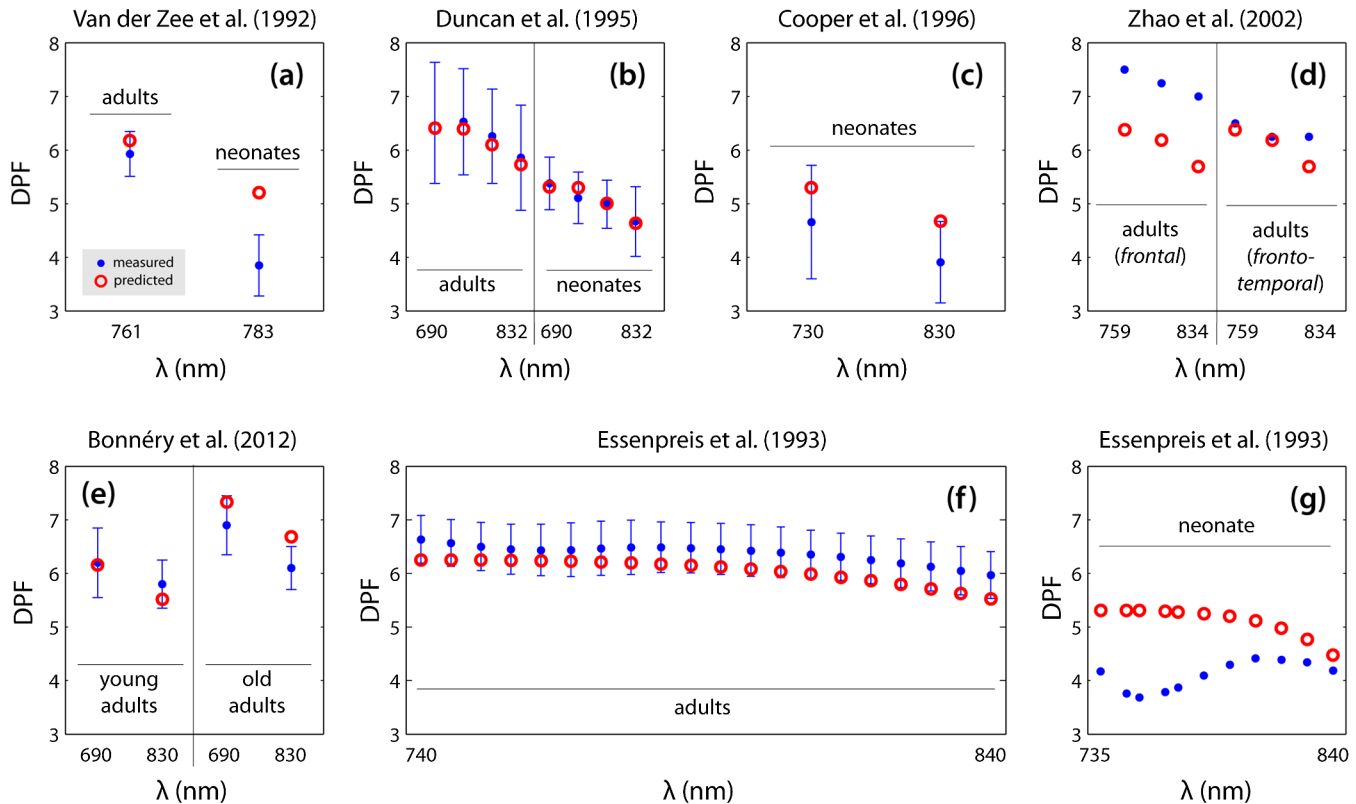


Fig. 3 (a–g) The five different data sets with measured DPF values [blue dots and error bars (if available)] and predicted DPF values (red dots). The error bars correspond to the standard deviation (SD) (a–c, f) or the quartiles (e).

predicted DPF for the adults agrees with the measured value. For the neonates, the predicted value was outside the SD range of the measured one. Since experimental data were not reported with SD values for the data set of Zhao et al.,²⁸ the agreement was only determined qualitatively. Two out of six values agreed. The agreement was greatest for the values from the frontotemporal region. Concerning the data set of Bonnéry et al.,²⁹ all four values agreed with the predicted ones.

For the Essenpreis et al.³⁰ data set of adults, the predicted DPF values agree with the measured ones. For the data set of a neonate also reported by Essenpreis et al., the predicted values differed from the measured ones. However, it must be noted that these data set originates only from one subject, making the decision of agreement difficult, especially in the region of approximately 800 to 840 nm where the measured and predicted values are close together and might coincide when more than one neonate had been measured and thus SD values were available.

In summary, excluding the data sets of Zhao et al. and the neonate data set of Essenpreis et al., 34 out of 36 values were correctly predicted. It should be noted that the data from the experimental studies show a relatively high degree of variability.

3 Discussion, Conclusion, and Outlook

We derived a general formula for the DPF depending on the wavelength and age based on the data of Duncan et al.¹⁵ For validation purposes, the derived formula was compared with (1) the values calculated by Eqs. (3)–(6) derived by Duncan et al. and (2) six independent data sets^{6,26–30} of measured DPF values from adults and neonates. The comparisons revealed that 34 out of 36 of the experimentally obtained values were predicted with satisfactory accuracy by the new equation, excluding

the data sets of Zhao et al.²⁸ and the neonate data set of Essenpreis et al.³⁰ where the validation was difficult since no SD values were given and only one subject was measured, respectively.

The discrepancy between the predicted and measured DPF values for the neonatal data sets of Van der Zee et al.⁶ and Essenpreis et al.³⁰ are likely due to the fact that the neonates were measured post mortem. In addition, the neonate measured by Essenpreis et al. was kept at 4°C prior to the measurement. Both death and low temperature influence the optical properties of the tissue. Our derived DPF equation is valid only for living humans. It is known that the optical properties of tissue are different for the *in vivo* and post mortem case³¹ although a study in rats found only a small change in the DPF upon death.³ Besides death, the cooling of the body is likely to influence the DPF measurement since a change in temperature has an effect on the optical properties of tissue.³²

As previous studies have shown, the DPF does not depend on skin color.²⁶ The dependence on gender is controversial.^{6,26} But as already shown by Zhao et al.,²⁸ the DPF depends clearly on the head region investigated. Therefore, to go one step further in the modeling of DPF values, it would be necessary to incorporate the dependency on the head region, i.e., composition of different tissue types, as a third variable, besides wavelength and age. It is known that variations in tissue type and the presence of the cerebral spinal fluid (CSF) have a significant effect on the light-propagation characteristics and thus the DPF.^{33–35} For example, Okada et al.³⁴ concluded that for a source–detector distance of 5 cm, the mean light propagation distance in the medium, i.e., d DPF, is composed of 65% contribution from the scalp and skull, 35% from the CSF, and 5% from the

GM. However, later works demonstrated that the light-piping effect of the CSF is reduced due to the presence of scattering structures, i.e., arachnoid trabeculae, within the CSF,^{36–38} reducing the influence of the CSF. To account for the mean pathlength in each tissue layer, the concept of the “partial differential pathlength” (also termed “partial optical path length”), i.e., the mean pathlength of the light in a specific layer, the “partial differential pathlength factor,” and the “partial pathlength factor,” were introduced.^{39–42}

Since the basis of the equation derived in this work comprises DPF values measured on the frontal and frontotemporal region, this equation is only valid for this head region. Another source of variation of the DPF is the intersubject variability indicating that the DPF varies by individual subject due to anatomical differences.⁴³ These factors might explain not only the discrepancy of the DPF prediction and the actual values as observed for the data sets of Van der Zee et al.⁶ and Zhao et al.²⁸ but also the discrepancy of reported experimentally obtained DPF values for the same age group, i.e., Van der Zee et al.⁶ versus Cooper et al.²⁷

Concerning the validity of the newly derived equation, we recommend its usage for the age range of 0 to 70 years and the wavelength range of 690 to 832 nm since it is derived from and validated using values in these ranges. For <690 nm, the equation is probably not correct due to a decrease of the DPF in this range.⁴⁴ It should be safe for application to values ranging from 832 nm to 950 nm because the wavelength dependence in this region should continue according to the model.⁴⁵

Acknowledgments

We thank Raphael Zimmermann, Andreas Metz, and Lisa Holper for discussions and manuscript reviews, and Rachel Scholkmann for proofreading of the manuscript.

References

1. M. Wolf, M. Ferrari, and V. Quaresima, “Progress of near-infrared spectroscopy and topography for brain and muscle clinical applications,” *J. Biomed. Opt.* **12**(6), 062104 (2007).
2. F. Scholkmann et al., “A review on continuous wave functional near-infrared spectroscopy and imaging instrumentation and methodology,” *Neuroimage* (2013), in press.
3. D. T. Delpy et al., “Estimation of optical pathlength through tissue from direct time of flight measurement,” *Phys. Med. Biol.* **33**(12), 1433–1442 (1988).
4. S. Fantini et al., “Non-invasive optical mapping of the piglet brain in real time,” *Opt. Express* **4**(8), 308–314 (1999).
5. D. A. Boas et al., “The accuracy of near infrared spectroscopy and imaging during focal changes in cerebral hemodynamics,” *Neuroimage* **13**(1), 76–90 (2001).
6. P. van der Zee et al., “Experimentally measured optical pathlengths for the adult head, calf and forearm and the head of the newborn infant as a function of inter optode spacing,” *Adv. Exp. Med. Biol.* **316**, 143–153 (1992).
7. P. van der Zee et al., “The effect of optode positioning on optical pathlength in near infrared spectroscopy of brain,” *Adv. Exp. Med. Biol.* **277**, 79–84 (1990).
8. S. Fantini et al., “Non-invasive optical monitoring of the newborn piglet brain using continuous-wave and frequency-domain spectroscopy,” *Phys. Med. Biol.* **44**(6), 1543–1563 (1999).
9. T. Talukdar, J. H. Moore, and S. G. Diamond, “Continuous correction of differential path length factor in near-infrared spectroscopy,” *J. Biomed. Opt.* **18**(5), 056001 (2013).
10. M. Kohl et al., “Separation of changes in light scattering and chromophore concentrations during cortical spreading depression in rats,” *Opt. Lett.* **23**(7), 555–557 (1998).
11. M. A. Franceschini, E. Gratton, and S. Fantini, “Noninvasive optical method of measuring tissue and arterial saturation: an application to absolute pulse oximetry of the brain,” *Opt. Lett.* **24**(12), 829–831 (1999).
12. A. Liebert et al., “Evaluation of optical properties of highly scattering media by moments of distributions of times of flight of photons,” *Appl. Opt.* **42**(28), 5785–5792 (2003).
13. A. Lieber, H. Wabnitz, and C. Elster, “Determination of absorption changes from moments of distributions of times of flight of photons: optimization of measurement conditions for a two-layered tissue model,” *J. Biomed. Opt.* **17**(5), 057005 (2012).
14. I. D. C. Tullis and D. T. Delpy, “Optical pathlength meter for near-infrared spectroscopy,” *Proc. SPIE* **4432**, 17–23 (2001).
15. A. Duncan et al., “Measurement of cranial optical path length as a function of age using phase resolved near infrared spectroscopy,” *Pediatr. Res.* **39**(5), 889–894 (1996).
16. S. Sgouros et al., “Intracranial volume change in childhood,” *J. Neurosurg.* **91**(4), 610–616 (1999).
17. W. Xing et al., “Probabilistic MRI brain anatomical atlases based on 1,000 Chinese subjects,” *PLoS One* **8**(1), e50939 (2013).
18. D. P. Carmody et al., “A quantitative measure of myelination development in infants, using MR images,” *Neuroradiology* **46**(9), 781–786 (2004).
19. A. Giorgio et al., “Age-related changes in grey and white matter structure throughout adulthood,” *Neuroimage* **51**(3), 943–951 (2010).
20. K. L. Leenders et al., “Cerebral blood flow, blood volume and oxygen utilization. Normal values and effect of age,” *Brain* **113**(1), 27–47 (1990).
21. D. G. Murphy et al., “Age-related differences in volumes of subcortical nuclei, brain matter, and cerebrospinal fluid in healthy men as measured with magnetic resonance imaging,” *Arch. Neurol.* **49**(8), 839–845 (1992).
22. D. D. Thompson, “Age changes in bone mineralization, cortical thickness, and haversian canal area,” *Calcif. Tissue Int.* **31**(1), 5–11 (1980).
23. R. W. Hill and P. W. Holland, “Two robust alternatives to least-squares regression,” *J. Am. Stat. Assoc.* **72**(360a), 828–833 (1977).
24. K. Levenberg, “A method for the solution of certain non-linear problems in least squares,” *Quart. J. Appl. Math.* **2**(2), 164–168 (1944).
25. D. Marquardt, “An algorithm for least-squares estimation of nonlinear parameters,” *SIAM J. Appl. Math.* **11**(2), 431–441 (1963).
26. A. Duncan et al., “Optical pathlength measurements on adult head, calf and forearm and the head of the newborn infant using phase resolved optical spectroscopy,” *Phys. Med. Biol.* **40**(2), 295–304 (1995).
27. C. E. Cooper et al., “The noninvasive measurement of absolute cerebral deoxyhemoglobin concentration and mean optical path length in the neonatal brain by second derivative near infrared spectroscopy,” *Pediatr. Res.* **39**(1), 32–38 (1996).
28. H. Zhao et al., “Maps of optical differential pathlength factor of human adult forehead, somatosensory motor and occipital regions at multi-wavelengths in NIR,” *Phys. Med. Biol.* **47**(12), 2075–2093 (2002).
29. C. Bonnéry et al., “Changes in diffusion path length with old age in diffuse optical tomography,” *J. Biomed. Opt.* **17**(5), 056002 (2012).
30. M. Essenpreis et al., “Spectral dependence of temporal point spread functions in human tissues,” *Appl. Opt.* **32**(4), 418–425 (1993).
31. B. C. Wilson, W. P. Jeeves, and D. M. Lowe, “In vivo and post mortem measurements of the attenuation spectra of light in mammalian tissues,” *Photochem. Photobiol.* **42**(2), 153–162 (1985).
32. J. Laufer et al., “Effect of temperature on the optical properties of ex vivo human dermis and subdermis,” *Phys. Med. Biol.* **43**(9), 2479–2489 (1998).
33. M. Firbank et al., “An investigation of light transport through scattering bodies with non-scattering regions,” *Phys. Med. Biol.* **41**(4), 767–783 (1996).
34. E. Okada et al., “Theoretical and experimental investigation of near-infrared light propagation in a model of the adult head,” *Appl. Opt.* **36**(1), 21–31 (1997).
35. E. Okada and D. T. Delpy, “Near-infrared light propagation in an adult head model. II. Effect of superficial tissue thickness on the sensitivity of the near-infrared spectroscopy signal,” *Appl. Opt.* **42**(16), 2915–2922 (2003).
36. E. Okada and D. T. Delpy, “Near-infrared light propagation in an adult head model. I. Modeling of low-level scattering in the cerebrospinal fluid layer,” *Appl. Opt.* **42**(16), 2906–2914 (2003).
37. E. Okada and D. T. Delpy, “Effect of scattering of arachnoid trabeculae on light propagation in the adult brain,” in *Proc. Biomedical Optical*

- Spectroscopy and Diagnostics*, T. Li, Vol. 38, p. ME3-1, Optical Society of America (2000).
38. Z. Rodriguez et al., "Experimental assessment of the CSF contribution to light propagation in the adult head," in *Conference on Lasers and Electro-Optics, CLEO '01*, pp. 401-402 (2001).
39. M. Hiraoka et al., "A Monte Carlo investigation of optical pathlength in inhomogeneous tissue and its application to near-infrared spectroscopy," *Phys. Med. Biol.* **38**(12), 1859-1876 (1993).
40. Y. Fukui, Y. Ajichi, and E. Okada, "Monte Carlo prediction of near-infrared light propagation in realistic adult and neonatal head models," *Appl. Opt.* **42**(16), 2881-2887 (2003).
41. K. Uludag et al., "Cross talk in the Lambert-Beer calculation for near-infrared wavelengths estimated by Monte Carlo simulations," *J. Biomed. Opt.* **7**(1), 51-59 (2002).
42. E. Okada et al., "Experimental validation of Monte Carlo and finite-element methods for the estimation of the optical path length in inhomogeneous tissue," *Appl. Opt.* **35**(19), 3362-3371 (1996).
43. M. Ferrari et al., "Variability of human brain and muscle optical pathlength in different experimental conditions," *Proc. SPIE* **1888**, 466-472 (1993).
44. G. Strangman, M. A. Franceschini, and D. A. Boas, "Factors affecting the accuracy of near-infrared spectroscopy concentration calculations for focal changes in oxygenation parameters," *Neuroimage* **18**(4), 865-879 (2003).
45. M. Kohl et al., "Determination of the wavelength dependence of the differential pathlength factor from near-infrared pulse signals," *Phys. Med. Biol.* **43**(6), 1771-1782 (1998).